

Supporting Information

Rational Fabrication of Defect-Rich and Hierarchically Porous Fe-N-C Nanosheets as Highly Efficient Oxygen Reduction Electrocatalysts for Zinc-Air Battery

Sensen Li, Yan Lv, Sawida Elam, Xiuli Zhang, Zhuojun Yang, Xueyan Wu * and Jixi Guo *

State Key Laboratory of Chemistry and Utilization of Carbon Based Energy Resources, College of Chemistry, Xinjiang University, Urumqi 830017, China

* Correspondence: wuxy90@xju.edu.cn (X.W.); jxguo1012@163.com (J.G.)

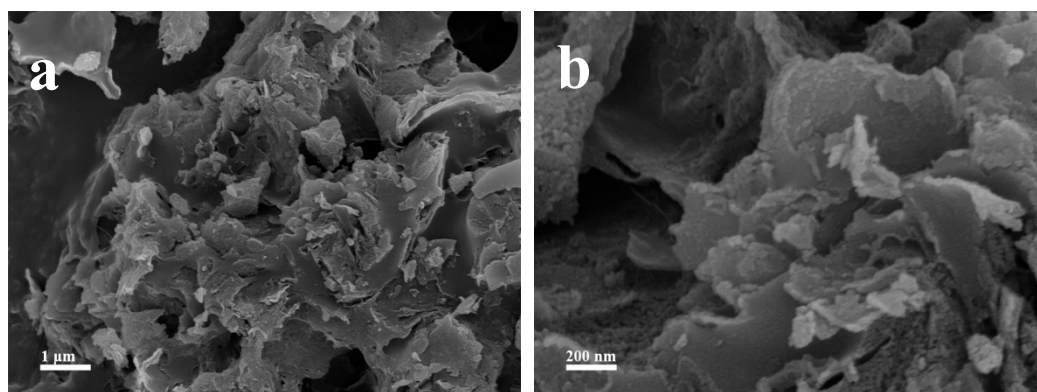


Figure S1. SEM images of Fe-N-CNSs-800.

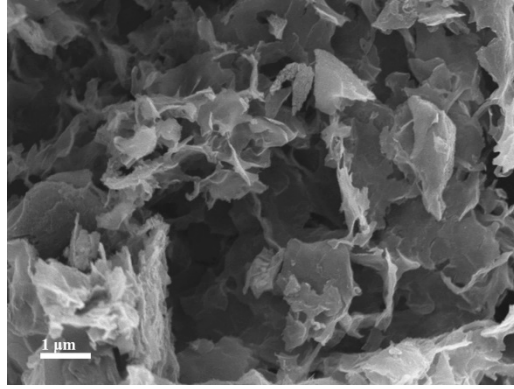


Figure S2. SEM image of Fe-N-CNSs-900.

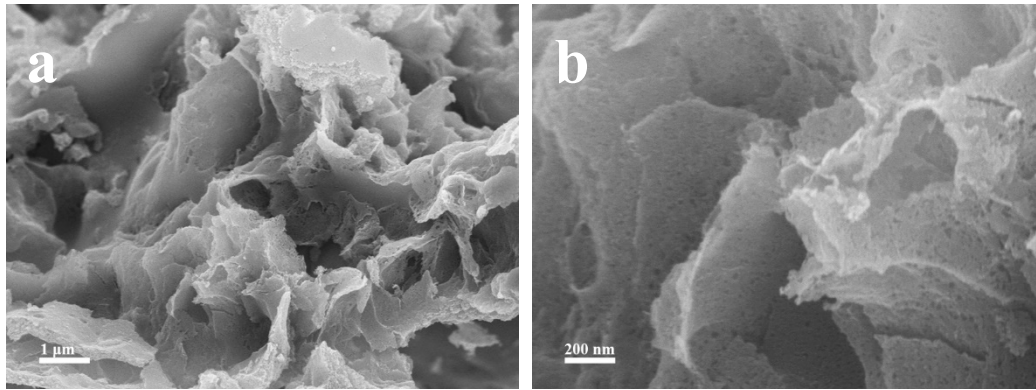


Figure S3. SEM images of Fe-N-CNSs-1000

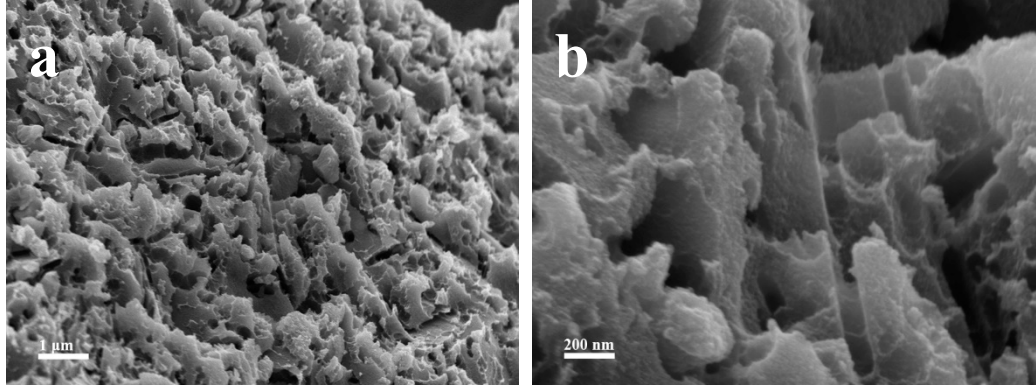


Figure S4. SEM images of Fe-N-C-900.

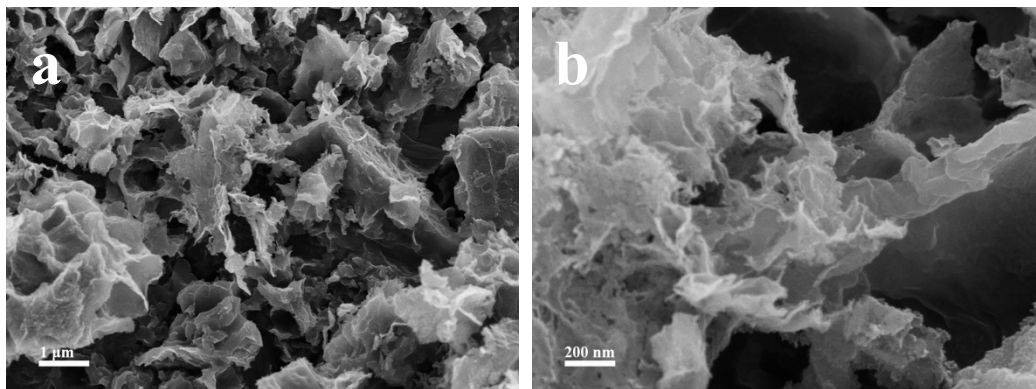


Figure S5. SEM images of Fe-N-CNSs-15.

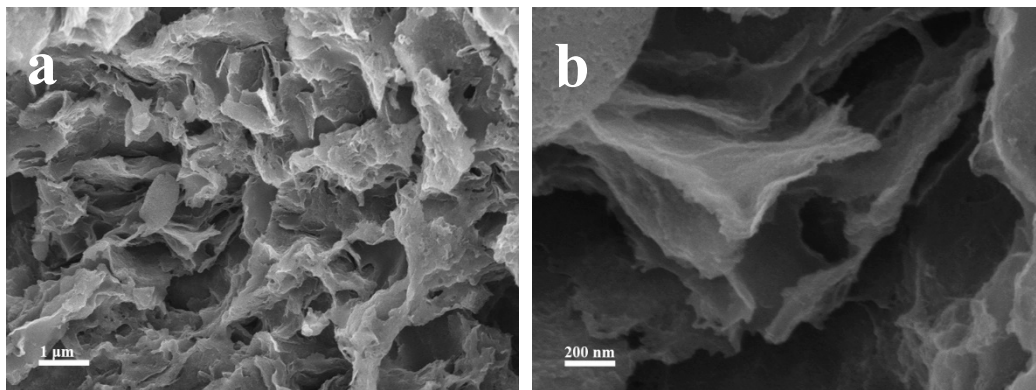


Figure S6. SEM images of Fe-N-CNSs-60.

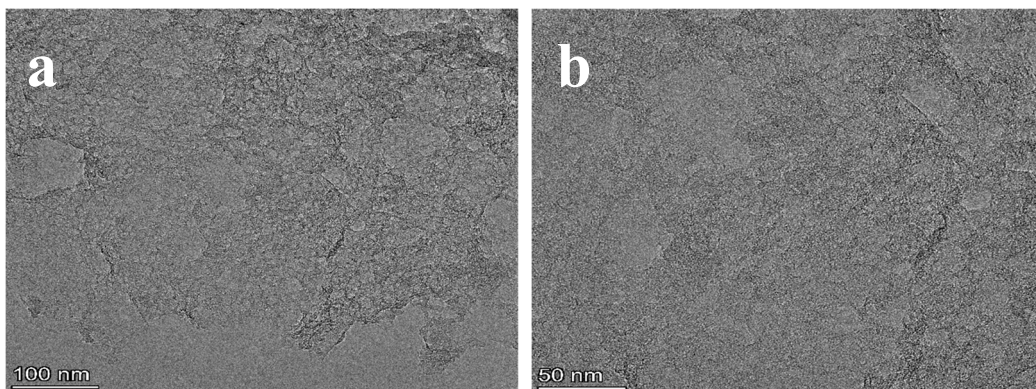


Figure S7. TEM images of Fe-N-CNSs.

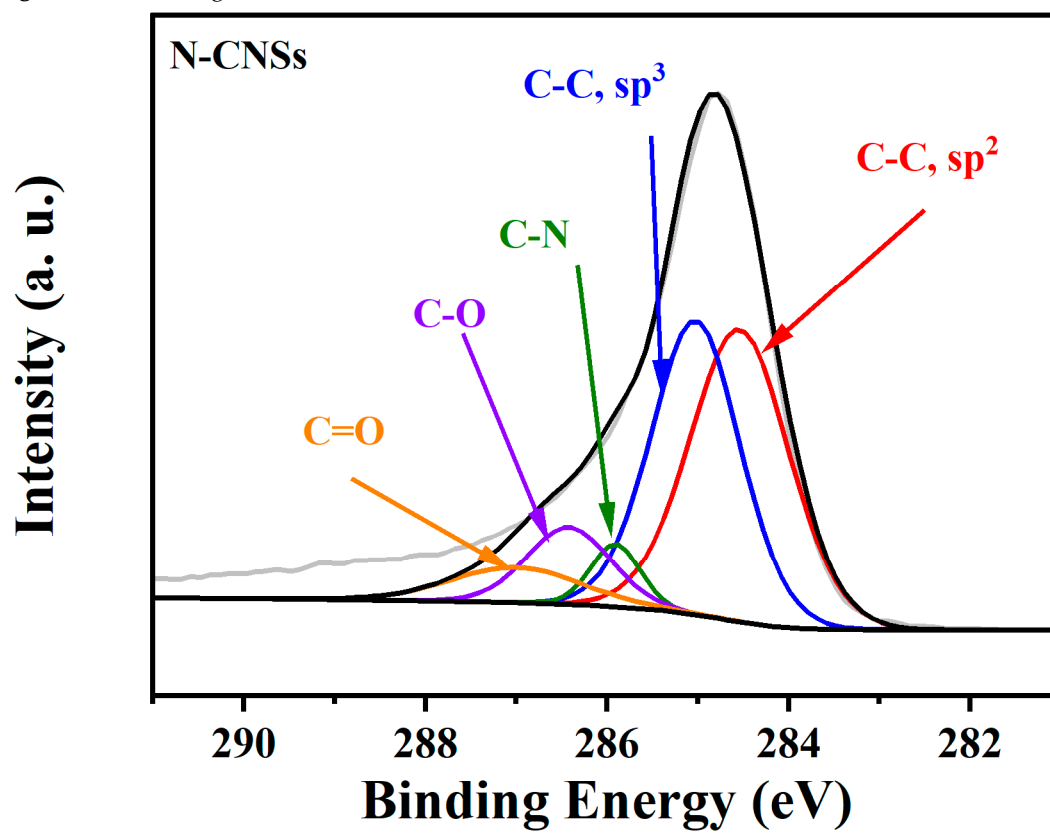


Figure S8. High-resolution C 1s spectrum of N-CNSs.

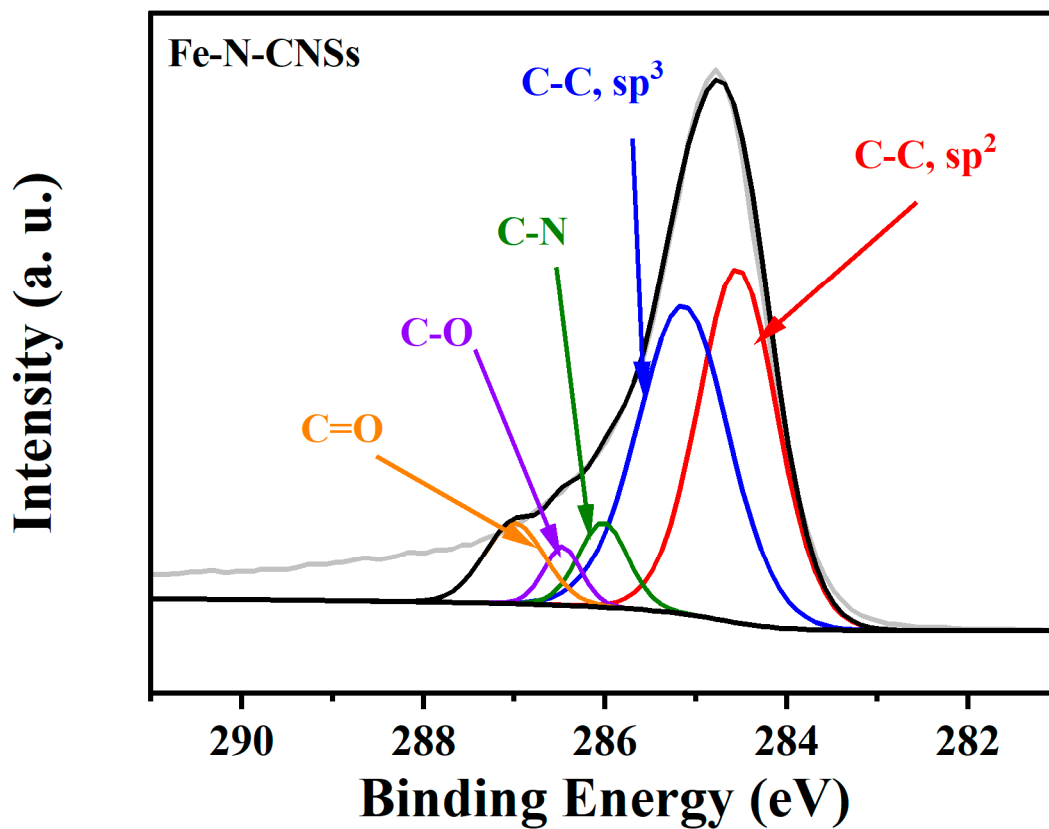


Figure S9. High-resolution C 1s spectrum of Fe-N-CNSs.

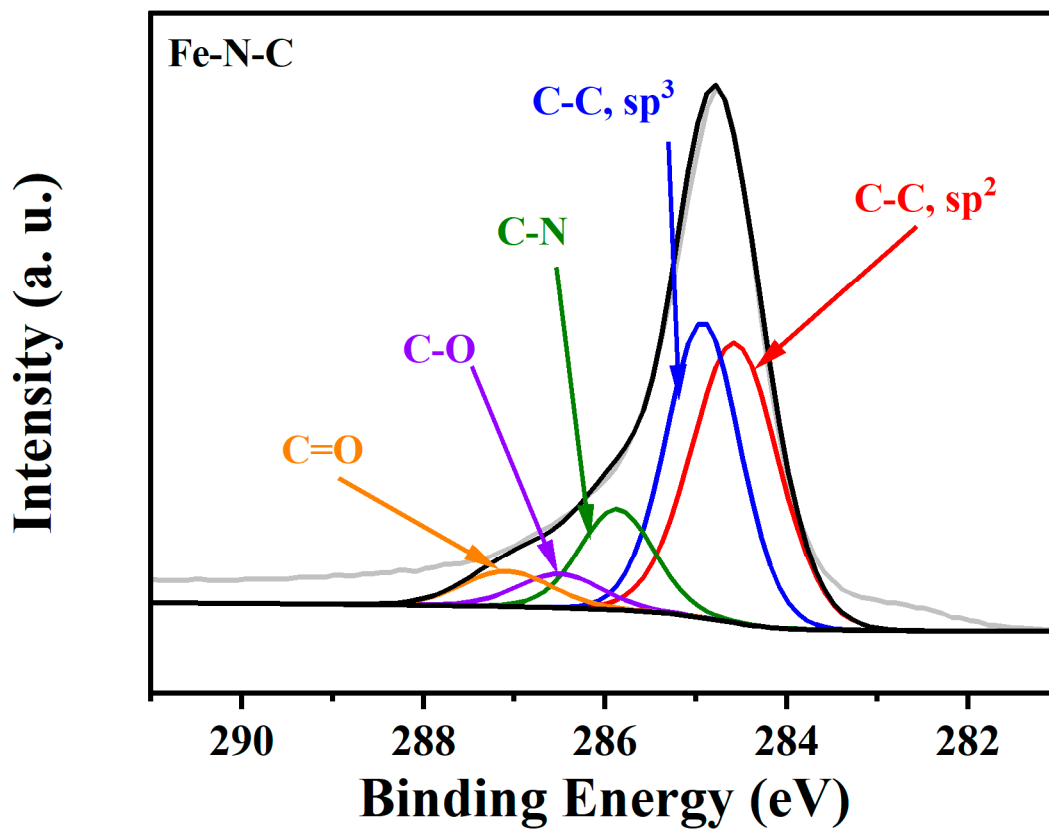


Figure S10. High-resolution C 1s spectrum of Fe-N-C.

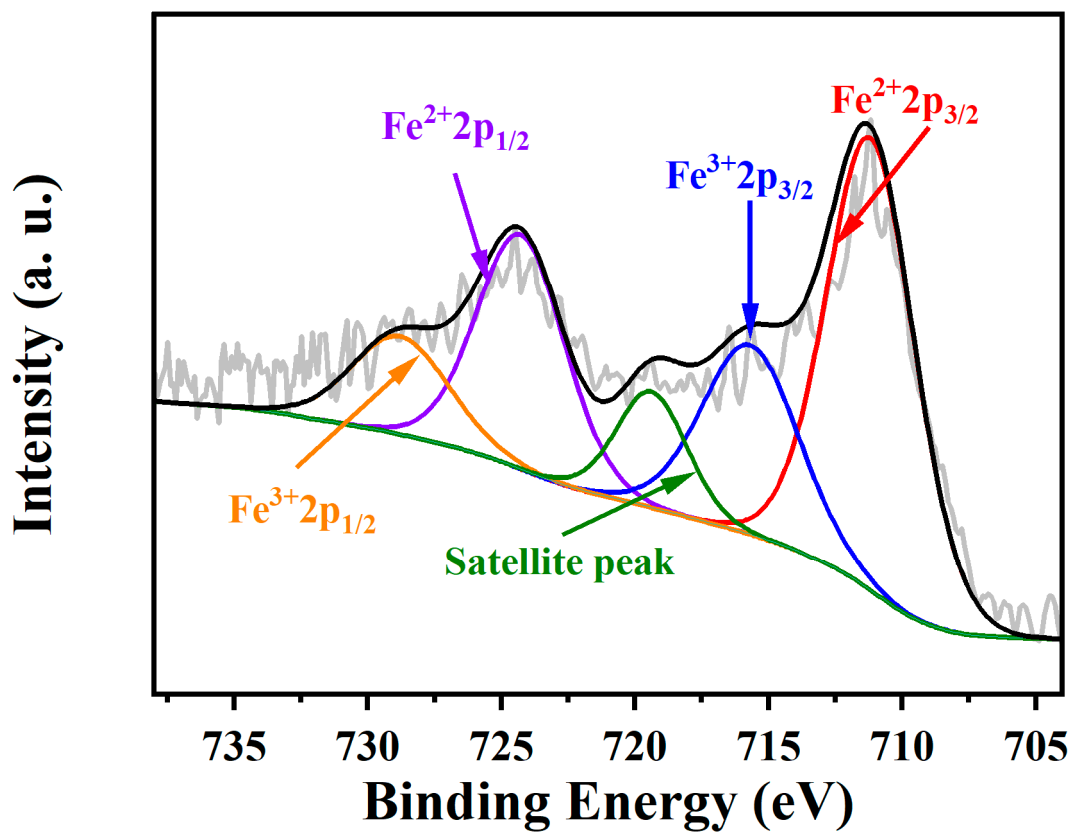


Figure S11. High-resolution Fe 2p spectrum of Fe-N-CNSs.

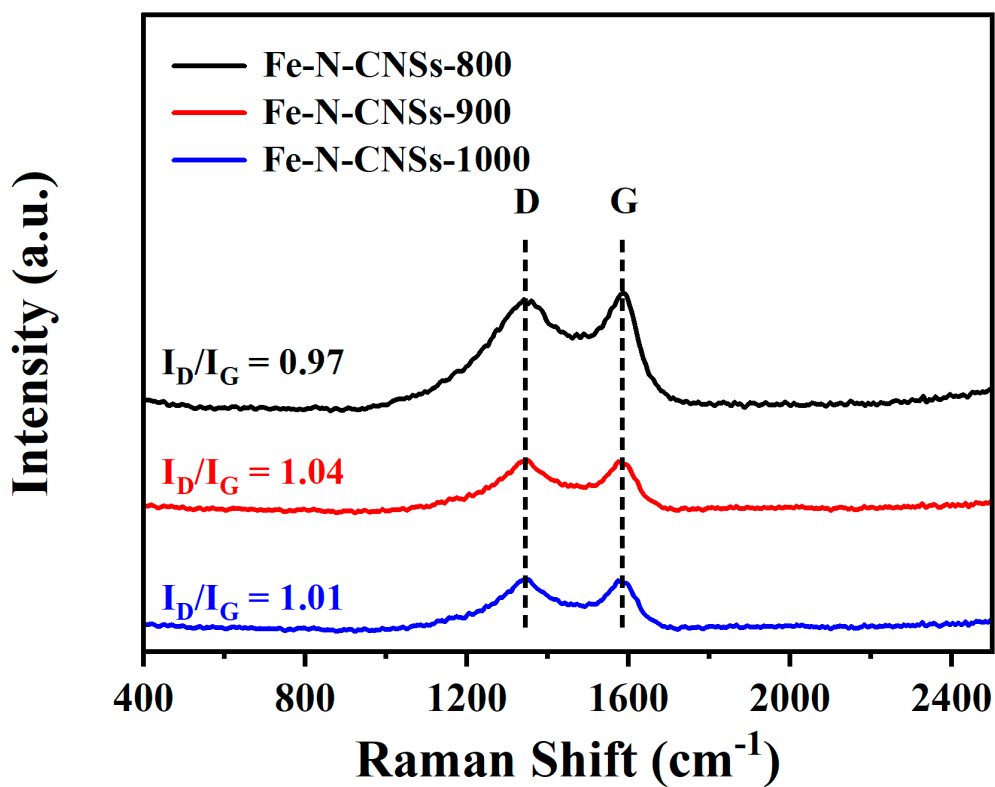


Figure S12. Raman spectra of the synthesized materials.

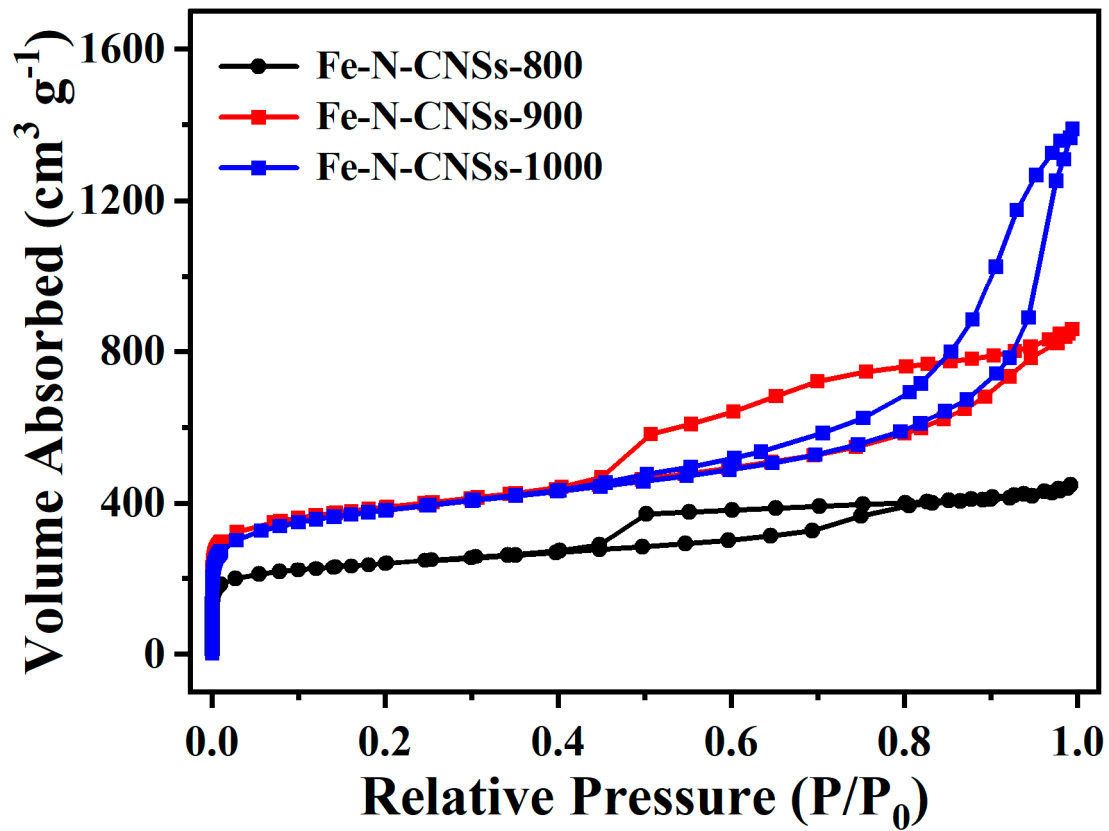


Figure S13. N_2 adsorption-desorption isotherms of Fe-N-CNSs-800, Fe-N-CNSs-900 and Fe-N-CNSs-1000.

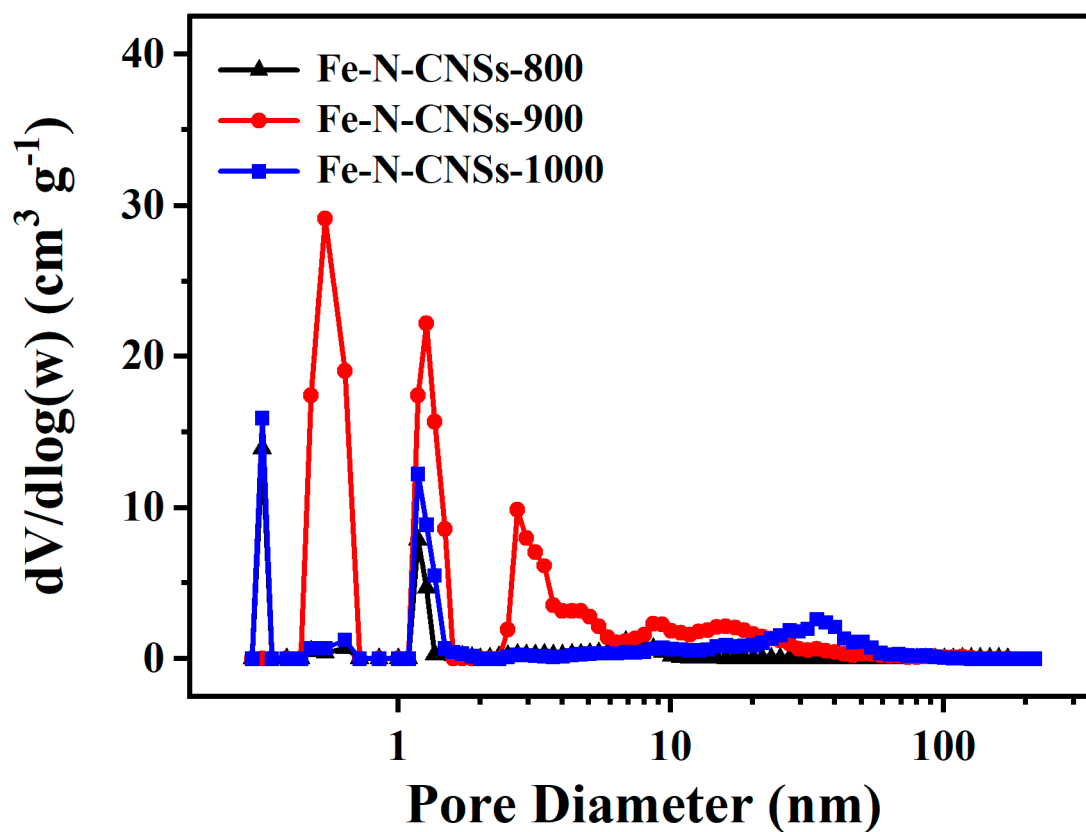


Figure S14. The pore size distribution of Fe-N-CNSs-800, Fe-N-CNSs-900 and Fe-N-CNSs-1000.

Table S1. Comparison of ORR activity of various Fe-N-C catalysts.

Catalysts	Electrolyte	$E_{1/2}$ (V vs. RHE)	Reference
Fe-N-CNSs	0.1 M KOH	0.87	This work
Fe-SAC/NC	0.1 M KOH	0.84	<i>Nano Energy</i> 2020 , 72, 104670.
Fe-N-C/NG	0.1 M KOH	0.84	<i>J. Alloy. Compd.</i> 2022 , 901, 163763.
Fe-AC-2	0.1 M KOH	0.87	<i>J. Mater. Chem. A</i> 2021 , 9, 7137–7142.
Fe-N-C/HPC-NH ₃	0.1 M KOH	0.80	<i>Nano Res.</i> 2019 , 12, 1651–1657.
AC-N-Fe	0.1 M KOH	0.76	<i>Chem. Eng. J.</i> 2022 , 446, 137256.
Fe-mela-mPD-N-C	0.1 M KOH	0.86	<i>J. Alloy. Compd.</i> 2023 , 935, 168069.
FeN ₄ -O-NCR	0.1 M KOH	0.94	<i>Adv. Mater.</i> 2022 , 34, 2202544.
Fe-N-C/MXene	0.1 M KOH	0.84	<i>ACS Nano</i> 2020 , 14, 2436–2444.
FeNSC-ZM	0.1 M KOH	0.87	<i>Chem. Eng. J.</i> 2022 , 444, 136433.

Fe/Meso-NC-1000	0.1 M KOH	0.88	<i>Adv. Mater.</i> 2022 , 34, 2107291.
SA Fe@ZrO ₂ /NC	0.1 M KOH	0.86	<i>Chem. Eng. J.</i> 2021 , 420, 129938.

Table S2. Comparison of the performance of the primary zinc-air batteries with the present work.

Catalysis	Peak power density (mW cm ⁻²)	Reference
Fe-N-CNSs	128.20	This work
IrFe-N-C	113.9	<i>ACS Catal.</i> 2022 , 12, 9397-9409
M-Fe-NCNSs	110.5	<i>Chem. Eng. J.</i> 2020 , 393, 124702
FeN _x /S-NC	83	<i>Appl. Surf. Sci.</i> 2022 , 580, 152255
Fe-N-C	167	<i>Nano Energy</i> 2022 , 104, 107869
FeNC	118.05	<i>Materials Today Energy</i> 2020 , 18, 100500
AC-N-Fe	124.2	<i>Chem. Eng. J.</i> 2022 , 446, 137256
P-Fe-N-CNTs	145	<i>Appl. Catal. B: Environ.</i> 2023 , 327, 122469
Fe ₃ -N-C-800	80	<i>New J. Chem.</i> 2022 , 46,989-994

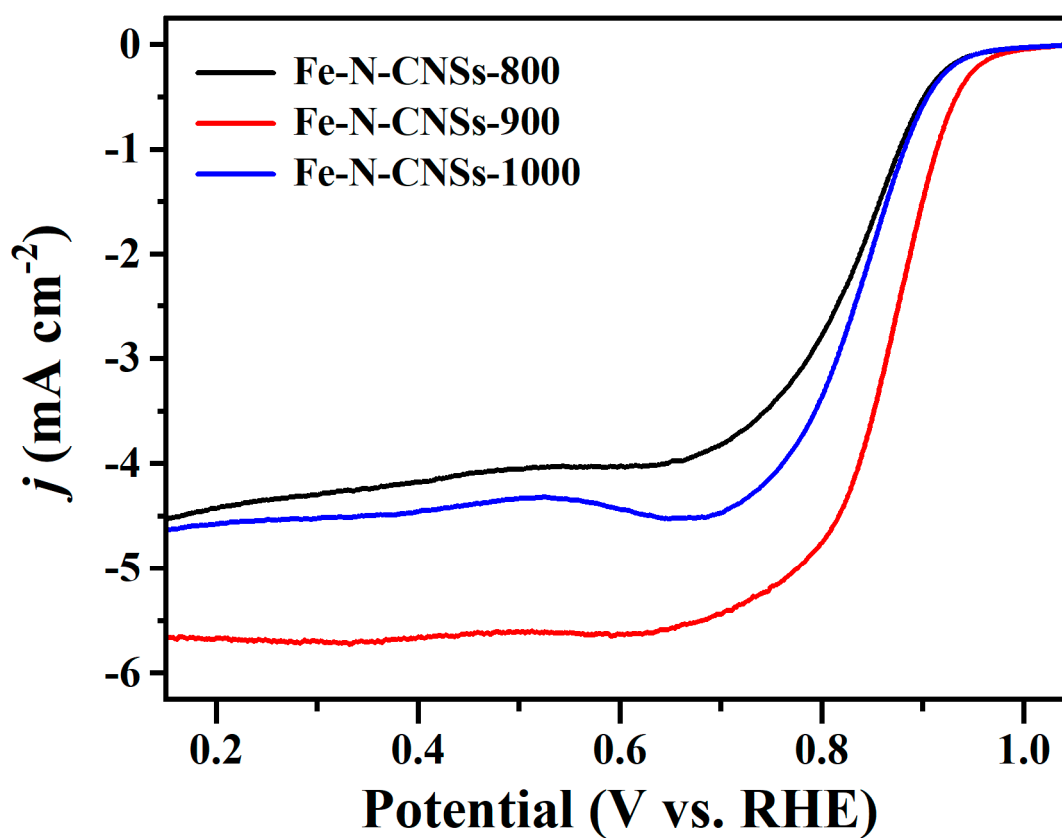


Figure S15. LSV curves of Fe-N-CNSs-800, Fe-N-CNSs-900, Fe-N-CNSs-1000.

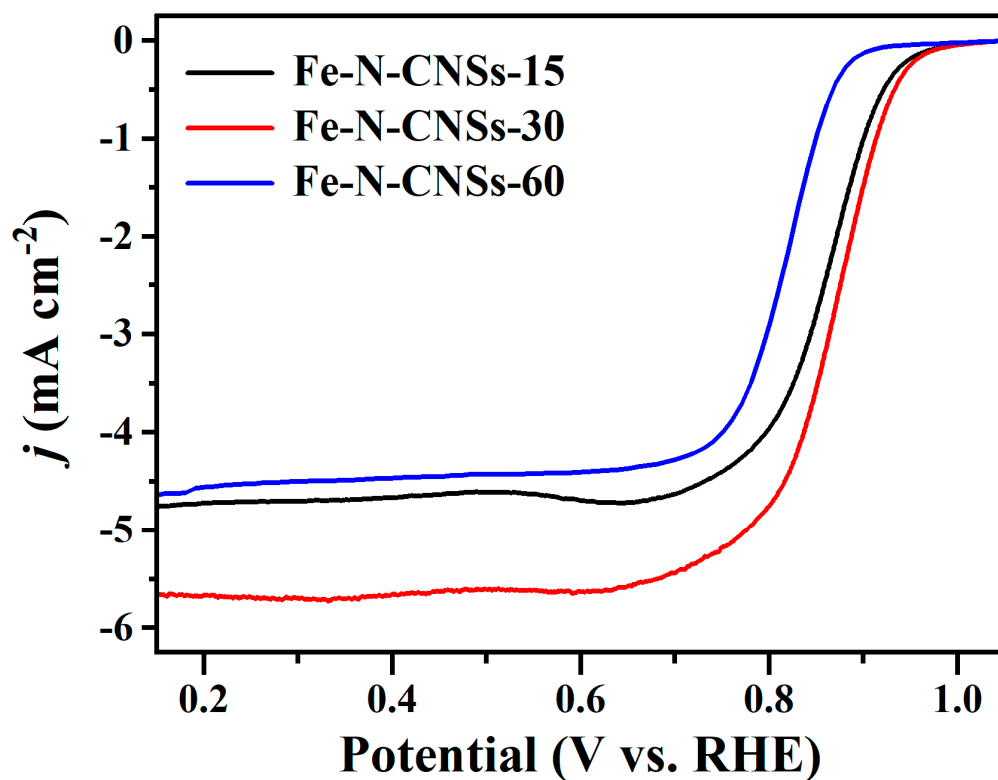


Figure S16. LSV curves of Fe-N-CNSs-15, Fe-N-CNSs-30, Fe-N-CNSs-60.

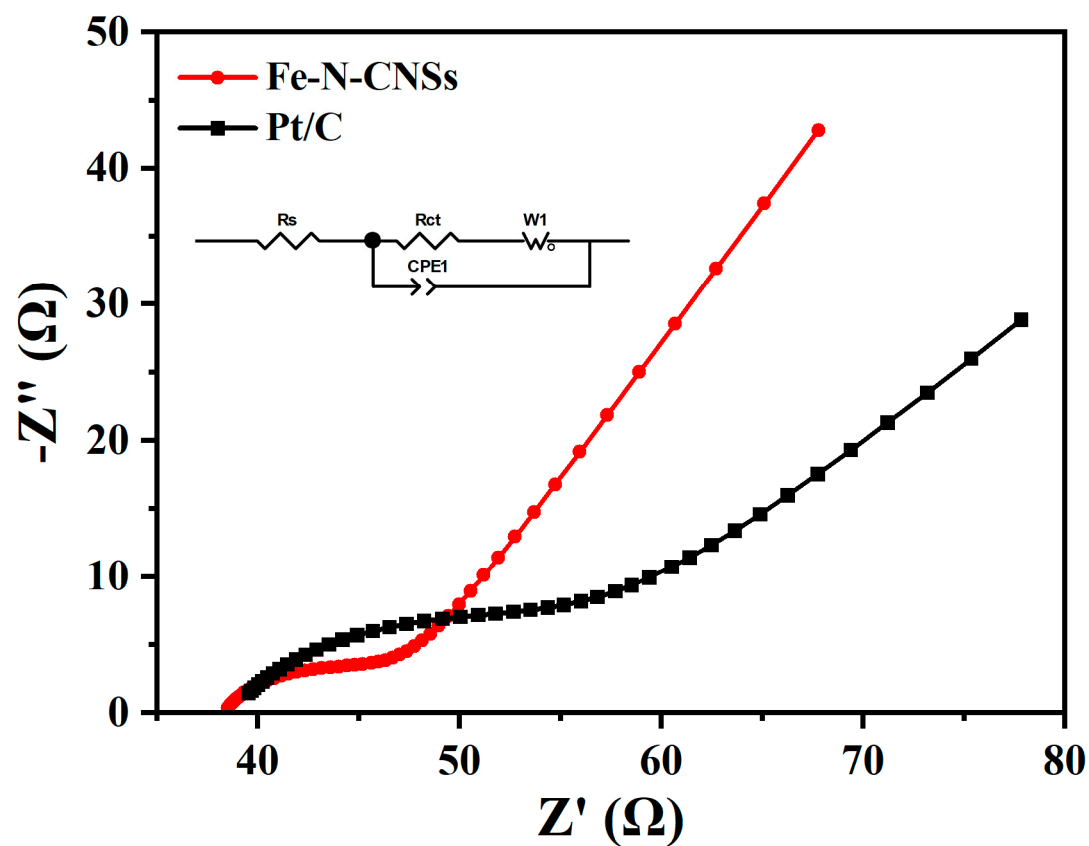


Figure S17. Nyquist plots of electrochemical impedance spectroscopy (EIS) for Fe-N-CNSs and Pt/C.

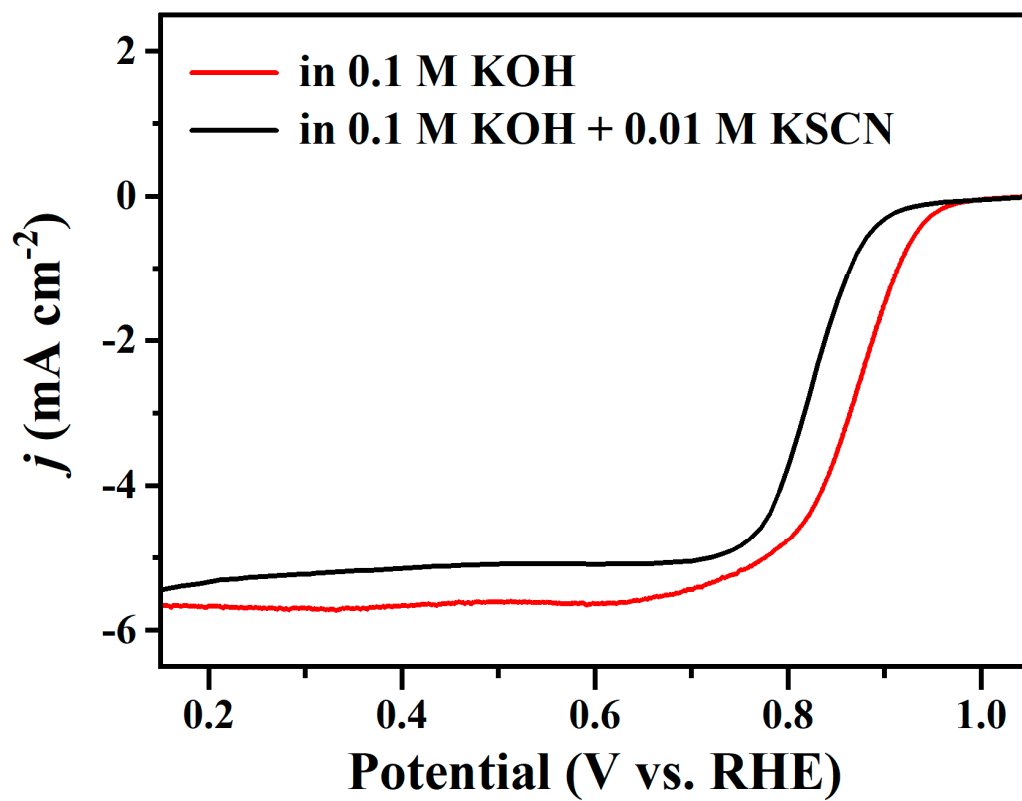


Figure S18. Poison experiment by KSCN.